2019 International Conference on Robotics and Automation (ICRA)
Palais des congres de Montreal, Montreal, Canada, May 20-24, 2019

Robotic Cutting: Mechanics and Control of Knife Motion

Xiaoqian Mu, Yuechuan Xue, and Yan-Bin Jia

Abstract— **Effectiveness of cutting is measured by the ability to achieve material fracture with smooth knife movements. The work performed by a knife overcomes the material toughness, acts against the blade-material friction, and generates shape deformation. This paper studies how to control a 2-DOF robotic arm equipped with a force/torque sensor to cut through an object in a sequence of three moves: press, push, and slice. For each move, a separate control strategy in the Cartesian space is designed to incorporate contact and/or force constraints while following some prescribed trajectory. Experiments conducted over several types of natural foods have demonstrated smooth motions like would be commanded by a human hand.**

I. INTRODUCTION

Automation of kitchen skills is an important part of home robotics, and also one of the ultimate tests for robots to achieve human-like dexterity. Despite its significance and appeal, until today robotic kitchen assistance has been limited to dish washing and sorting, and to cooking of food items prepared by human. The Moley Robotic Kitchen [1], the world's first of its kind, only memorizes and replicates exact movements of a human chef. Meanwhile, in factory settings, robotic systems are typically for one type of task, whether cutting meat, deboning, or butchering chicken.

Cutting skills such as chop, slice, and dice are mostly beyond the reach of today's robots. Technical challenges come not just from manipulation of soft and irregularly-shaped objects, but more from doing so while fracture is happening. The latter requires planning and force control based on reliable modeling of an object's deformation and fracture as it is being cut. The knife's movement needs to be adjusted to progress in terms of material fracture. Its trajectory may need to be replanned in the case of an unforeseeable situation (e.g., appearance of a bone).

*Support for this research has been provided by the US National Science Foundation under Grant IIS-1651792. Any opinions, findings, and conclusions or recommendations expressed in this material are those of the authors and do not necessarily reflect the views of the National Science Foundation.

*We would like to thank labmate Prajjwal Jamdagni for discussion and for his help with fracture toughness measurements.

The authors are with the Department of Computer Science, Iowa State University, Ames, IA 50011, USA muxiao, yuechuan, jia@iastate.edu

Cutting is a process during which the knife needs to respond to reaction forces due to different sources (fracture, friction, contact) that are exerted by the material throughout the action and also by the cutting board for some period of time. Although the goal is steady progress leading to complete separation of the material, changing contacts, kinematics, and path constraints require different periods of cutting to carry specific control objectives. In this paper, we will accordingly present a sequence of hybrid control policies to ensure the completion.

II. RELATED WORK

Fracture mechanics [2] builds on a balance between the work done by cutting and the total amount spent for crack propagation, transformed into other energy forms (strain, kinetic, chemical, etc.), and dissipated by friction. Methods for measuring fracture toughness were surveyed for ductile materials [3] and presented for live tissue [4]. Stress and fracture force analyses, supported by simulation and experiment, were performed on robotic cutting of bio-materials, while accounting for factors such as blade sharpness and slicing angle [5], [6], [7]. A "slice/push ratio" was introduced in [8] to quantitatively characterize the dramatic decrease in the cutting force when the knife is "pressing and slicing". By incorporating this ratio, the cutting force and torque could be obtained via an integration along the edge of the blade [9]. This method is also used in our paper. We refer to [10] for a survey on mechanics and modeling of cutting biological materials.

In surgical training, realistic haptic display of soft tissue cutting is quite important. A haptic model for scissor cutting of animal tissue was created [11]. Other efforts were on modeling of soft tissue deformation prior to fracture for haptic display [12], as well as on understanding the mechanics of needle insertion into soft tissue [13]. Most approaches in this area tended to be empirical.

Force control [14] is the default for robustly dealing with modeling and position errors in contact tasks. Impedance control [15] adjusts contact force from a motion deviation like an intended mass-spring-damper. Cutting, nevertheless, intends to fracture the object

978-1-5386-6026-3/19/$31.00 ©2019 IEEE

rather than exhibit certain impedance to it. Robotic cutting has been investigated in a number of ways: adaptive control based on position and velocity history to learn the applied force [16], adaptive force tracking via impedance control [17], visual servoing coupled with force control [18], and cooperation of a cutting robot for trajectory following and a pulling robot under impedance control [19].

Keeping the knife orientation during cutting reduces to control of a constrained manipulator [20, pp. 202-203]. To deal with contact constraints, controls of force and position are more effectively conducted in the workspace [21] using a reduced set of coordinates [22, pp. 501-510]. Hybrid force/position control [23] is a natural choice when the knife is slicing through an object while maintaining contact with the cutting board.

III. MECHANICS OF CUTTING

In this paper, a vector is represented by a lowercase letter in bold, e.g, $\boldsymbol{a} = (a_x, a_y)^T$, with its x- and y-coordinates denoted by the same (non-bold) letter with subscripts x and y, respectively. A unit vector has a hat, e.g., $\hat{\boldsymbol{a}} = \boldsymbol{a}/\|\boldsymbol{a}\|$. The cross product $\boldsymbol{a} \times \boldsymbol{b}$ of two vectors $\boldsymbol{a}$ and $\boldsymbol{b}$ is treated as a scalar. The dot ‘˙’ is used for differentiation with respect to time.

As shown in Fig. 1, cutting takes place in the vertical x-y plane (the *world frame*) located at $\boldsymbol{o}$ on the cutting board. From now on, all vectors will be described in this frame by default unless specifically mentioned. The knife's blade remains in the x-y plane during cutting. Attached to the knife point $\boldsymbol{k}$ is a local frame x'-y', called the *knife frame*, which is rotated through an angle θ_k from the world frame.

In the x'-y' frame, the knife's edge and spine are described by two curves $\boldsymbol{\beta}_k(u) = (\beta_{kx}, \beta_{ky})^T$ and $\boldsymbol{\gamma}_k(q) = (\gamma_{kx}, \gamma_{ky})^T$, respectively, such that $\boldsymbol{\beta}_k(0)$ and $\boldsymbol{\gamma}_k(0)$ coincide with $\boldsymbol{k}$. In the world frame, the edge and spine are described by the following two curves:

$$\boldsymbol{\beta}(u) = (\beta_x, \beta_y)^T = \boldsymbol{k} + R(\theta_k)\boldsymbol{\beta}_k(u), \quad (1)$$

$$\boldsymbol{\gamma}(q) = \boldsymbol{k} + R(\theta_k)\boldsymbol{\gamma}_k(q), \quad (2)$$

where $R(\theta_k)$ is the rotation matrix for the knife.

At the start of cutting (time $t = 0$), the edge contacts the object at a single point. Later on, it intersects the object at a section of $\boldsymbol{\beta}(u)$ over the interval $[u_1, u_2]$, $u_1 \le u_2$. The section, shown in Fig. 1, is also denoted $\boldsymbol{\beta}[u_1, u_2]$. A section of the spine $\boldsymbol{\gamma}(q)$ over, say, $[q_1, q_2]$, may also be inside the object.

Given the slow cutting speed, we can make the following assumption:

(A1) The dynamic effects on the object are insignificant.

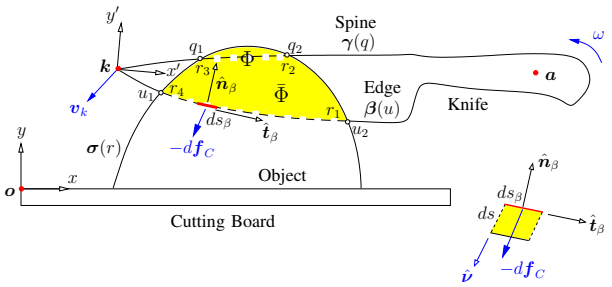

Fig. 1. Geometry and mechanics of cutting.

Some foods like potatoes and yams barely deform during cutting. In this paper, we will relieve ourselves from deformable modeling with a second assumption:

(A2) The material being cut has negligible deformation.

Since the object does not deform, we let the curve $\boldsymbol{\sigma}(r)$ describe its non-varying cross section intersected by the x-y plane. The knife's edge intersects the curve at $\boldsymbol{\sigma}(r_4)$ and $\boldsymbol{\sigma}(r_1)$ from left to right. The segments $\boldsymbol{\beta}[u_1, u_2]$ and $\boldsymbol{\sigma}[r_1, r_4]$ enclose the *fracture region* Φ. When a section of the spine $\boldsymbol{\gamma}[q_1, q_2]$ is inside the cross section, the four segments $\boldsymbol{\beta}[u_1, u_2]$, $\boldsymbol{\sigma}[r_1, r_2]$, $\boldsymbol{\gamma}[q_1, q_2]$, and $\boldsymbol{\sigma}[r_3, r_4]$ bound the *contact region* $\bar{\Phi}$, as illustrated in Fig. 1. Clearly, $\bar{\Phi} \subseteq \Phi$.

During cutting, the force exerted on the knife is $\boldsymbol{f} = \boldsymbol{f}_C + \boldsymbol{f}_F$, where $\boldsymbol{f}_C$ and $\boldsymbol{f}_F$ are called fracture and frictional forces, respectively. The work done by $-\boldsymbol{f}_C$ yields new fracture while that by $-\boldsymbol{f}_F$ is dissipated through friction.[1]

Consider an infinitesimal element of length ds_β on the knife's edge starting at $u \in [u_1, u_2]$ (see Fig. 1). The element may or may not be generating fracture under the knife's rotation. We need only focus on the former case here. Let $\boldsymbol{v}_k$ be the velocity of the knife point $\boldsymbol{k}$, and ω the knife's angular velocity. The element exerts the force $-d\boldsymbol{f}_C$ in the direction of its velocity $\boldsymbol{\nu} = \boldsymbol{v}_k + \omega \binom{-\beta_{ky}}{\beta_{kx}}$ to generates an area of fracture that is a parallelogram illustrated on the lower right in Fig. 1. Its four sides are parallel to either the edge tangent $\hat{\boldsymbol{t}}_\beta$ or the velocity $\boldsymbol{\nu}$. Let $\hat{\boldsymbol{n}}_\beta$ be the unit normal of the knife's edge at $\boldsymbol{\beta}(u)$. Denote by κ the material's fracture toughness[2]. We have $(-d\boldsymbol{f}_C \cdot \hat{\boldsymbol{\nu}})ds = -\kappa(\hat{\boldsymbol{\nu}} \cdot \hat{\boldsymbol{n}}_\beta) ds ds_\beta$, which leads to

$$d\boldsymbol{f}_C = \kappa(\hat{\boldsymbol{\nu}} \cdot \hat{\boldsymbol{n}}_\beta)\hat{\boldsymbol{\nu}}\, ds_\beta = \kappa \left(\hat{\boldsymbol{\nu}} \cdot \left(-\frac{d\beta_y}{du}, \frac{d\beta_x}{du} \right)^T \right) \hat{\boldsymbol{\nu}}\, du.$$

[1]For a deformable object, the equation's right hand side also includes $\boldsymbol{f}_U$, where the work by $-\boldsymbol{f}_U$ causes an increase (or decrease) in the object's strain energy.

[2]energy required to propagate a crack by unit area [2, p. 16]

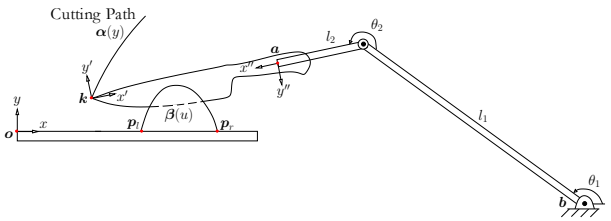

Fig. 2. Pressing by translating the knife downward.

Integration over the segment $S = \boldsymbol{\beta}[u_1, u_2]$ yields the total force $\boldsymbol{f}_C$ contributing to fracture:

$$\boldsymbol{f}_C = \int_S d\boldsymbol{f}_C. \tag{3}$$

The knife is rigidly attached to a robotic arm's free end $\boldsymbol{a}$,[3] which receives a torque exerted by the object:

$$\tau_C = \int_S (\boldsymbol{\beta}(u) - \boldsymbol{a}) \times d\boldsymbol{f}_C. \tag{4}$$

Coulomb friction exists in the contact region $\bar{\Phi}$, on both sides of the blade. Let P be the pressure distribution and μ the coefficient of friction. Denote by $\hat{\boldsymbol{v}}(x, y)$ the direction of the velocity of an area element at $(x, y)^T$ inside the contact region $\bar{\Phi}$. The force and torque at the open end $\boldsymbol{a}$ due to friction are given below:

$$\boldsymbol{f}_F = -2\mu P \iint_{\bar{\Phi}} \hat{\boldsymbol{v}}\, dxdy, \tag{5}$$

$$\tau_F = -2\mu P \iint_{\bar{\Phi}} \left(\begin{pmatrix} x \\ y \end{pmatrix} - \boldsymbol{a} \right) \times \hat{\boldsymbol{v}}\, dxdy. \tag{6}$$

Given the knife's pose $(\boldsymbol{k}, \theta_k)$ the wrenches $(\boldsymbol{f}_C, \tau_C)$ and $(\boldsymbol{f}_F, \tau_F)$ can be evaluated.

IV. DYNAMICS AND CONTROL OF CUTTING

As shown in Fig. 2, the robotic arm has two links of lengths l_1 and l_2 moving in the x-y plane. The corresponding two joint angles are denoted by θ_1 and θ_2. The arm's base is located at $\boldsymbol{b}$. At its free end $\boldsymbol{a}$ is attached a frame x''-y'' referred to as the *arm frame*.

Besides causing fracture and overcoming friction, the arm needs to balance the knife's gravitational force and its resulting torque. The wrench (force and torque) exerted at $\boldsymbol{a}$ due to cutting, friction, and knife gravity is

$$\boldsymbol{w}_a = \begin{pmatrix} \boldsymbol{f}_C + \boldsymbol{f}_F - m_k g \hat{\boldsymbol{y}} \\ \tau_C + \tau_F - m_k g (\boldsymbol{c}_k - \boldsymbol{a}) \times \hat{\boldsymbol{y}} \end{pmatrix}, \tag{7}$$

where m_k is the knife's mass, $\boldsymbol{c}_k$ the location of its center of mass, $g > 0$ the gravitational acceleration, and $\hat{\boldsymbol{y}} = (0, 1)^T$. Denote $\boldsymbol{\theta} = (\theta_1, \theta_2)^T$, $\theta_a = \theta_1 + \theta_2$,

[3]A force/torque (F/T) sensor is located at the open end and regarded as part of the arm's last link.

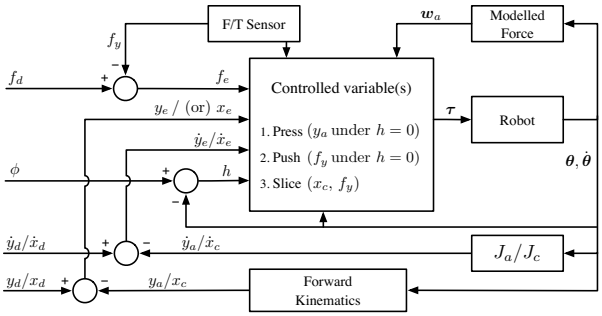

Fig. 3. Control diagram for three cutting phases.

$\hat{\boldsymbol{l}}_1 = \binom{\cos\theta_1}{\sin\theta_1}$, and $\hat{\boldsymbol{l}}_2 = \binom{\cos\theta_a}{\sin\theta_a}$. The Jacobian for $\boldsymbol{a}$ is a 3×2 matrix:

$$J_a = \frac{\partial}{\partial \boldsymbol{\theta}} \begin{pmatrix} l_1 \hat{\boldsymbol{l}}_1 + l_2 \hat{\boldsymbol{l}}_2 \\ \theta_a \end{pmatrix} \tag{8}$$

such that $(\dot{\boldsymbol{a}}^T, \dot{\theta}_a)^T = J_a \dot{\boldsymbol{\theta}}$.

Cutting of an object proceeds in three phases. The first phase is *pressing*, during which the arm translates the knife downward until its edge touches the cutting board. The second (transitional) phase is *pushing* during which the arm continues pressing the knife downward until the contact force reaches a desired level. The third phase is *slicing* during which the arm translates and rotates the knife to move its contact point with the cutting board across the object's bottom segment $\overline{\boldsymbol{p}_l \boldsymbol{p}_r}$ in the cutting plane. The object is then split into two parts.

A. Pressing

In this phase, the arm dynamics are as follows:

$$J_a^T \boldsymbol{w}_a + \boldsymbol{\tau} = M(\boldsymbol{\theta})\ddot{\boldsymbol{\theta}} + C(\boldsymbol{\theta}, \dot{\boldsymbol{\theta}})\dot{\boldsymbol{\theta}} + V(\boldsymbol{\theta}), \tag{9}$$

where $\boldsymbol{\tau}$ is the joint torque vector, $M(\boldsymbol{\theta})$ is the arm's 2×2 mass matrix, $C(\boldsymbol{\theta}, \dot{\boldsymbol{\theta}})\dot{\boldsymbol{\theta}}$ includes the Coriolis and centrifugal terms, and $V(\boldsymbol{\theta})$ is the gravity term. The arm frame's orientation is kept at some constant angle ϕ so the knife does not rotate, that is,

$$h(\boldsymbol{\theta}) \equiv \phi - (\theta_1 + \theta_2) = 0. \tag{10}$$

Under the above constraint, the arm's free end is at

$$\boldsymbol{a} = (x_a, y_a)^T = l_1 \hat{\boldsymbol{l}}_1 + l_2 \hat{\boldsymbol{l}}_2. \tag{11}$$

Hence, $\boldsymbol{a}$ moves on a circular arc parameterized in y_a.

We can choose y_a as the new coordinate with $\boldsymbol{\theta} = \boldsymbol{\theta}(y_a)$ defined by (10). The Jacobian for this coordinate transformation is $\boldsymbol{l}_a = \partial\boldsymbol{\theta}/\partial y_a = (d\theta_1/dy_a, -d\theta_1/dy_a)^T$, where $d\theta_1/dy_a$ is obtained from differentiating the second equation in (11). Substituting $\dot{\boldsymbol{\theta}} = \boldsymbol{l}_a \dot{y}_a$ and $\ddot{\boldsymbol{\theta}} = \dot{\boldsymbol{l}}_a \dot{y}_a + \boldsymbol{l}_a \ddot{y}_a$ into (9), we rewrite the dynamics in the Cartesian space:

$$\boldsymbol{\tau} = M \boldsymbol{l}_a \ddot{y}_a + N_a, \tag{12}$$

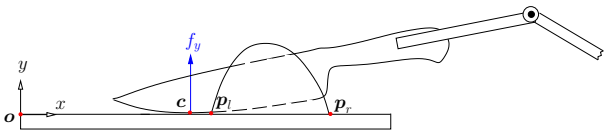

Fig. 4. Establishing contact with the cutting board.

where $N_a = (M\dot{\boldsymbol{l}}_a + C\boldsymbol{l}_a)\dot{y}_a + V - J_a^T\boldsymbol{w}_a$ includes the Coriolis, centrifugal, and gravity effects, and the external wrench $\boldsymbol{w}_a$ (directly measured by the F/T sensor).

We intend to realize some desired trajectory $y_d(t)$ for y_a. At time $t = 0$, the knife's edge makes contact with the object at $y_d(0) = y_0$, which can be determined from the initial configuration. We also set $\bar{y}_1$ to a value of y_a at which the lowest point on the knife's edge is slightly into the cutting board. Then, we let $y_d(\bar{t}_1) = \bar{y}_1$ at time $\bar{t}_1 > 0$. Construct $y_d(t)$ based on the values of $y_d(0)$, $y_d(\bar{t}_1)$ and trapezoid velocity profile $\dot{y}_d(t)$. The condition $\dot{y}_d(\bar{t}_1) = 0$ intends to minimize the impact between the knife and the cutting board.

Let $y_e = y_d - y_a$ be the position error. We use a hybrid strategy with PID controls over both position and force:

$$\boldsymbol{\tau} = M\boldsymbol{l}_a\left(\ddot{y}_d + k_v\dot{y}_e + k_p y_e + k_i\int y_e\,dt\right) + N_a + F_a. \tag{13}$$

where $F_a = (h + k_{fd}\dot{h} + k_{fi}\int h\,dt)\nabla h^T$ is a generalized constraint force that performs no work by acting against any deviation of $h(\boldsymbol{\theta})$ from zero, i.e., any rotation of the knife. Equate (13) with (12), and then multiply both sides of the resulting closed-loop dynamics with $\boldsymbol{l}_a^T$ by making use of $\boldsymbol{l}_a^T\nabla h^T = (\nabla h\boldsymbol{l}_a)^T = 0$ (which follows from differentiating $h(\boldsymbol{\theta}) = 0$). This yields the position error dynamics:

$$\ddot{y}_e + k_v\dot{y}_e + k_p y_e + k_i\int y_e\,dt = 0,$$

where the gains k_v, k_p, k_i are properly selected.

B. Pushing

Pressing ends at time t_1 with a detection of contact between the knife's edge and the cutting board from a sudden increase in the force reading by the F/T sensor. The point of contact $\boldsymbol{c} = (x_c, y_c)^T$ can be made to lie initially to the left endpoint $\boldsymbol{p}_l$ (see Fig. 4). To cut through the object, the knife needs to maintain some force on the board. Since the knife's edge is very sharp, it is reasonable to make a third assumption:

(A3) No contact friction exists between the knife's edge and the cutting board.

We employ a different controller to regulate the upward contact force, represented by a scalar f_y (equivalently, the downward force $-f_y$ exerted by the knife on the board), at some constant value f_d. Due to this contact force, the dynamics have changed from (12) to

$$\boldsymbol{\tau} = M\boldsymbol{l}_a\ddot{y} + N_a - J_c^T(0, f_y)^T, \tag{14}$$

where $J_c = \partial\boldsymbol{k}/\partial\boldsymbol{\theta} + (\partial R(\theta_k)/\partial\boldsymbol{\theta})\boldsymbol{\beta}_k(u)$ (u treated as a constant) is the Jacobian of $\boldsymbol{c}$. For this phase, we employ a controller modified over (13):

$$\boldsymbol{\tau} = N_a + F_a + F_c, \tag{15}$$

where $F_c = -J_c^T\left(0, f_d + \bar{k}_{fd}\dot{f}_e + \bar{k}_{fi}\int f_e\,dt\right)^T$. Equate (15) with (14), and then multiply both sides with $\boldsymbol{l}_a^T$ to eliminate F_a. The term $\boldsymbol{l}_a^T M\boldsymbol{l}_a$ is positive since M is positive definite. The derivative $dy_c/dy_a = 1$, since the knife keeps a constant orientation. The error dynamics,

$$\boldsymbol{l}_a^T M\boldsymbol{l}_a\ddot{y}_e - 2\frac{dy_c}{dy_a}(f_e + \bar{k}_{fd}\dot{f}_e + \bar{k}_{fi}\int f_e\,dt) = 0 \tag{16}$$

will drive f_e to zero if the linear model $f_e = -K_e y_e$, where K_e is the environment stiffness, is applied and the values of $\bar{k}_{fd}$ and $\bar{k}_{fi}$ are properly set.

The sensor reading combines the wrench $\boldsymbol{w}_a$ at the arm's free end $\boldsymbol{a}$ due to cutting as well as the wrench at the knife-board contact $\boldsymbol{c}$. The value of f_y can be obtained from the sensor reading and the value of $\boldsymbol{w}_a$ from modeling. The derivative of f_y needed for applying (15) can be estimated from a curve fit to a sequence of previous values of f_y.

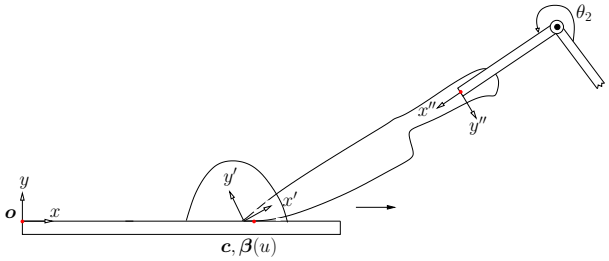

Fig. 5. Slicing along the cutting board.

C. Slicing

When the contact force f_y approaches f_d at some time t_2, the knife begins to slide rightward on the table to split the object. This is illustrated in Fig. 5. Let φ be the angle of rotation from the arm frame x''-y'' to the knife frame x'-y'. The knife undergoes a rotation of $\theta_k = \theta_1 + \theta_2 + \varphi$ from the world frame. Its point is at $\boldsymbol{k} = \boldsymbol{b} + l_1\hat{\boldsymbol{l}}_1 + l_2\hat{\boldsymbol{l}}_2 + R(\theta_k)\boldsymbol{k}''$, where $\boldsymbol{k}''$ is its (fixed) position in the arm frame.

It follows from (1) that the moving edge curve $\boldsymbol{\beta}$ depends on θ_k, and therefore on $\boldsymbol{\theta}$. We write $\boldsymbol{\beta}$ as

$\boldsymbol{\beta}(\boldsymbol{\theta}, u)$, with the value of u locating the instantaneous point $\boldsymbol{c}$ of contact. This point is also at $(x_c, 0)^T$. Thus,

$$\beta_x = x_c, \quad (17)$$
$$\beta_y = 0. \quad (18)$$

Meanwhile, $\boldsymbol{c}$ is the lowest point on $\boldsymbol{\beta}$, yielding

$$\frac{\partial \beta_y}{\partial u} = 0. \quad (19)$$

Equations (17)–(19) define θ_1, θ_2, and u as functions of x_c. Given x_c, we can solve for θ_1, θ_2, and u using Newton's method or the homotopy continuation method [24].

Meanwhile, equations (18) and (19) together define a curve $\boldsymbol{\theta}(u) = (\theta_1(u), \theta_2(u))^T$ in the joint space, which ensures the knife to stay in contact with the table as it moves. This curve has an implicit form $\rho(\boldsymbol{\theta}) = 0$. Such constraint allows us to introduce a new coordinate, conveniently, x_c, to replace $\boldsymbol{\theta}$, since the rest of cutting reduces to moving the point $(x_c, 0)^T$ from $\boldsymbol{p}_l$ to $\boldsymbol{p}_r$.

The Jacobian for the coordinate transformation is $\boldsymbol{l}_c = d\boldsymbol{\theta}/dx_c$. This derivative, along with du/dx_c, can be solved from the three linear equations generated from differentiating (17)–(19) with respect to x_c.

The dynamics are now described by

$$\boldsymbol{\tau} = M\boldsymbol{l}_c\ddot{x}_c + N_c - J_c^T(0, f_y)^T. \quad (20)$$

where $N_c = (M\dot{\boldsymbol{l}}_c + C\boldsymbol{l}_c)\dot{x} + V - J_a^T\boldsymbol{w}_a$. To evaluate $\dot{\boldsymbol{l}}_c = (d^2\boldsymbol{\theta}/dx_c^2)\dot{x}_c$, we obtain $d^2\theta_i/dx_c^2$, $i = 1, 2$, along with d^2u/dx_c^2 from differentiating (18) and (19) twice, utilizing the earlier obtained first derivatives of $\boldsymbol{\theta}$ and u.

Let $x_d(t)$ be some desired time trajectory of x_c with constant speed (hence $\ddot{x}_d = 0$). Let $x_e(t) = x_d - x_c$ be the position error of the contact point $\boldsymbol{c}$. The desired constant normal force on the table is still $-f_d$, so is the force error $f_e = f_d - f_y$. We apply a third control law:

$$\boldsymbol{\tau} = M\boldsymbol{l}_c\left(\bar{k}_v\dot{x}_e + \bar{k}_p x_e + \bar{k}_i\int x_e\,dt\right) + N_c + F_c, \quad (21)$$

where F_c was introduced in Section IV-B.

We can establish $\boldsymbol{l}_c^T J_c^T \binom{0}{1} = (0, 1)J_c\boldsymbol{l}_c = 0$ by showing that the latter product is a multiple of $(\partial\beta_y/\partial\boldsymbol{\theta}) \cdot (d\boldsymbol{\theta}/du)$, which can be proved to be zero from differentiating (18) with respect to u, with θ_1 and θ_2 treated as its functions, and then substituting (19). The identity allows us to multiply $\boldsymbol{l}_c^T$ with both sides of the closed loop dynamics from combining (20) and (21) to get rid of the force control term. The position error dynamics are obtained as

$$\ddot{x}_e + \bar{k}_v\dot{x}_e + \bar{k}_p x_e + \bar{k}_i\int x_e\,dt = 0.$$

Substituting the above into the closed loop dynamics, we obtain

$$f_d + \bar{k}_{fd}\dot{f}_e + \bar{k}_{fi}\int f_e\,dt = 0.$$

V. EXPERIMENTS

Fig. 6 shows the experiment setup. The arm used for cutting was a 4-DOF Whole Arm Manipulator (WAM) from Barrett Technology, LLC. Its joints 1 and 3 were fixed so the robot effectively had two DOFs. We derived the arm dynamics (9) according to the arm specifications[4]. A 6-axis force/torque sensor (Delta IP65) from ATI Industrial Automation was mounted on the end-effector of the robot arm.

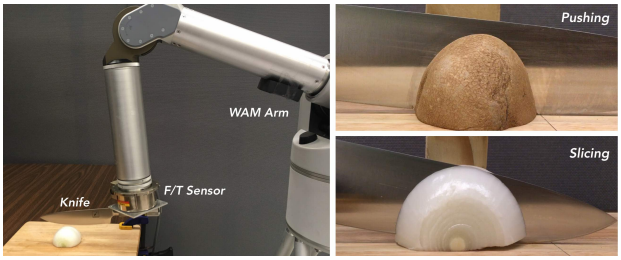

Fig. 6. Experiment setup.

To model a kitchen knife, we placed it on a sheet of paper, and drew its contour. The knife's edge $\boldsymbol{\beta}_k(u)$ was reconstructed in the knife frame x'-y' with u be the x'-coordinate. Then fit a polynomial curve β_{ky} to the y'-coordinates of the measured points on the edge. Similarly, the knife's spine was reconstructed through fitting as the polynomial curve $\boldsymbol{\gamma}_k(q) = (q, \gamma_{ky}(q))^T$ with q identified with x'.

Potatoes and onions were used in the experiment. In a trial, half of a potato or onion (cut by the human hand) was placed on a table with its flat face down, as shown in Fig. 6.[5] We used a Microsoft Kinect sensor to obtain points on the surface of the object, and fit over those "close enough" to the cutting plane to construct the contour $\boldsymbol{\sigma}(r)$, where r is the x-coordinate in the world frame.

The coefficients of friction between the knife and the cross section of the onion and the potato were measured to be 0.477 and 0.7, respectively. To measure the fracture toughness and pressure distribution, we let the robot move the knife to cut into each object and then lift it up with constant low speed. The pressure

[4] http://web.barrett.com/support/WAM_Documentation/WAM_InertialSpecifications_AC-02.pdf

[5] During cutting, we stabilized the object by pressing it with a piece of wood.

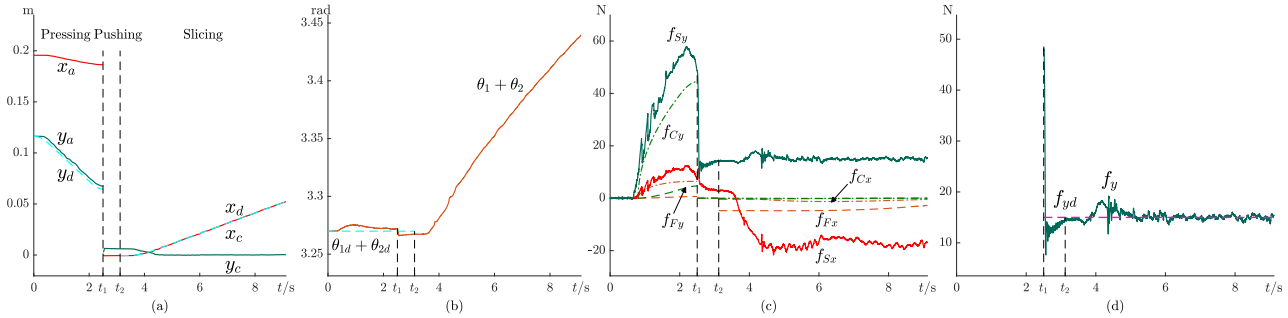

Fig. 7. Results from onion cutting. Trajectories of the (a) arm's free end $\boldsymbol{a}$ and contact point $\boldsymbol{c}$, (b) sum of the two joint angles, (c) force $\boldsymbol{f}_S = (f_{Sx}, f_{Sy})^T$ exerted on the knife as obtained from sensor readings, modeled fracture force $\boldsymbol{f}_C = (f_{Cx}, f_{Cy})^T$, and modeled frictional force $\boldsymbol{f}_F = (f_{Fx}, f_{Fy})^T$, and (d) contact force between the knife and cutting board in the y-direction.

distribution was obtained from the measurement of the F/T sensor and contact area in the lifting phase and the fracture toughness was calculated after subtracting the frictional force from the sensor reading of the cutting phase. The calculated values of pressure distribution were $2900N/m^2$ and $2000N/m^2$, of fracture toughness were $675J/m^2$ and $200J/m^2$ for the onion and potato, respectively. Controller gains were chosen based on earlier trials.

Low-pass filter was applied to velocities through cutting to weaken the effect of high frequency noise and to commanded torque in the transitions among the three phases to avoid sudden changes which could cause undesired oscillations of the arm.

Fig. 7 shows the experimental results from cutting an onion. Each of (a)–(d) illustrates all three phases of cutting. In (a), the ordinate y_a of the arm's free end follows the desired trajectory y_d during pressing, and the abscissa x_c of the knife-board contact point follows the desired trajectory x_d during slicing. In (b), the orientation $\theta_1 + \theta_2$ of the arm frame (hence that of the knife) stays almost constant in the first two phases, but increases in the third phase. In (c), the modeled frictional force $\boldsymbol{f}_F$ and fracture force $\boldsymbol{f}_C$ add up close to the sensed force $\boldsymbol{f}_S$ in the pressing phase, except every time the knife enters a new layer in the onion. In the slicing phase, the modeled force in the y-direction is very small, since every point on the knife is moving almost in the x-direction. In (d), a sudden change in the contact force has been caused by a large gap between the desired force and actual force. The contact force converges quickly to the desired value and varies within a small range.

Convergence to the desired knife motions were also observed in potato cutting. An instance is shown in Fig. 8.

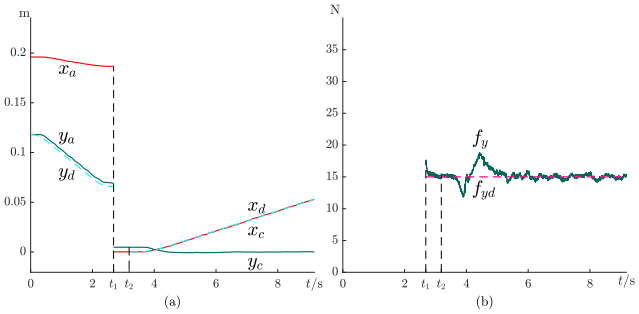

Fig. 8. Results for potato cutting. Trajectories of the (a) arm's free end $\boldsymbol{a}$ and contact point $\boldsymbol{c}$, and (b) contact force between the knife and cutting board in the y-direction.

VI. FUTURE WORK

Our next step will be to cut objects that will undergo visible deformations. A vision system will be used for tracking the object's shape but not its strain energy. For planning of cutting motion and real-time plan adjustment, it is very important to have reliable predictions of fracture and strain energy along a cutting trajectory. Accurately enough deformable modeling will allow tracking of the areas of fracture and contact. Though fracture modeling remains very challenging, there is room for inaccuracies which we hope can be compensated with force sensing and improved knife control strategies.

We would also like to use another robotic hand to pick up soft and leafy objects, and stabilize them during the cutting. A challenge would be its coordination with the arm that performs the cutting. Later on, we will look into issues of planning trajectories to implement different knife skills including chop, slice, and dice.

REFERENCES

[1] http://www.techinsider.io/moley-to-present-the-worlds-first-robot-kitchen-in-2017-2015-11.

[2] T. Atkins. *The Science and Engineering of Cutting*. Elsevier, Oxford OX2 8DP, UK, 2009.

[3] A. G. Atkins. "Toughness and cutting: a new way of simultaneously determining ductile fracture toughness and strength," *Engr. Fracture Mechanics*, vol. 72, pp. 850–860, 2004.

[4] C. Gokgol, C. Basdogan, and D. Canadinc. "Estimation of fracture toughness of liver tissue: Experiments and validation," *Medical Engr. Phy.*, vol. 34, pp. 882–891, 2012.

[5] D. Zhou, M. R. Claffee, K.-M. Lee, and G. V. McMurray. "Cutting, 'by pressing and slicing', applied to robotic cutting bio-materials, Part I: Modeling of stress distribution," in *Proc. IEEE/RSJ Int. Conf. Intell. Robots Syst.*, 2006, pp. 2896–2901.

[6] D. Zhou, M. R. Claffee, K.-M. Lee, and G. V. McMurray. "Cutting, 'by pressing and slicing', applied to robotic cutting bio-materials, Part II: Force during slicing and pressing cuts," in *Proc. IEEE/RSJ Int. Conf. Intell. Robots Syst.*, 2006, pp. 2256–2261.

[7] D. Zhou and G. McMurray. "Modeling of blade sharpness and compression cut of biomaterials," *Robotica*, vol. 28, pp. 311–319, 2010.

[8] A. G. Atkins, X. Xu, and G. Jeronimidis. "Cutting, by 'pressing and slicing,' of thin floppy slices of materials illustrated by experiments on cheddar cheese and salami," *J. Materials Sci.*, vol. 39, pp. 2761–2766, 2004.

[9] A. G. Atkins and X. Xu. "Slicing of soft flexible solids with industrial applications," *Int. J. Mech. Sci.*, vol. 47, pp. 479–492, 2005.

[10] B. Takabi and B. L. Tai. "A review of cutting mechanics and modeling techniques for biological materials," *Medical Engr. Phys.*, 45:1–14, 2017.

[11] V. Chial, S. Greenish, and A. M. Okamura. "On the display of haptic recordings for cutting biological tissues," in *HAPTICS*, 2002, pp. 80–87.

[12] T. Chanthasopeephan, J. P. Desai, and A. C. W. Lau. "Modeling soft-tissue defomration prior to cutting for surgical simulation: Finite analysis and study of cutting parameters," *IEEE Trans. Biomed. Engr.*, vol. 54, no. 3, pp. 349–359, 2007.

[13] M. Khadem, C. Rossa, R. S. Sloboda, N. Usmani, and M. Tavakoli. "Mechanics of tissue cutting during needle insertion in biological tissue," *IEEE Robot. Autom. Letters*, vol. 1, no. 2, pp. 800–807, 2016.

[14] L. Villani and J. D. Schutter. "Force Control," "in *Handbook of Robotics, Part A*, B. Siciliano and O. Khatib (eds.), Springer, pp. 195-219, 2008.

[15] N. Hogan. "Impedance control: An approach to manipulation: Parts I–III" *ASME J. Dynamic. Sys. Measure. Control*, vol. 107, pp. 1–24, 1985.

[16] G. Zeng and A. Hemami. "An adaptive control strategy for robotic cutting," in *Proc. IEEE Int. Conf. Robot. Autom.*, 1997, pp. 22–27.

[17] S. Jung and T. C. Hsia. "Adaptive force tracking impedance control of robot for cutting nonhomogeneous workpiece," in *Proc. IEEE Int. Conf. Robot. Autom.*, 1999, pp. 1800–1805.

[18] P. Long, W. Khalil, and P. Martinet. "Force/vision control for robotic cutting of soft materials," in *Proc. IEEE/RSJ Int. Conf. Intell. Robots Syst.*, 2014, pp. 4716–4721.

[19] P. Long, W. Khalil, and P. Martinet. "Modeling and control of a meat-cutting robotic cell," in *Proc. Int. Conf. Advanced Robot.*, 2013, pp. 61–66.

[20] R. M. Murray and Z. Li and S. S. Sastry. *A Mathematical Introduction to Robotic Manipulation*. CRC Press, Boca Raton, FL, 1994.

[21] O. Khatib. "A unified approach for motion and force control of robot manipulators: The operational space formulation," *IEEE J. Robot. Autom.*, vol. 3, pp. 43–53, 1987.

[22] F. L. Lewis and D. M. Dawson and C. T.Abdallah. *Robot Manipulator Control: Theory and Practice*, 2nd ed.. Marcel Dekker, Inc., 2004.

[23] M. Raibert and J. Craig. "Hybrid position/force control of manipulators", *ASME J. Dynamic. Sys. Measure. Control.*, vol. 103, no. 2, pp. 126–133, 1981.

[24] C. B. Garcia and W. I. Zangwill. "Finding all solutions to polynomial systems and other systems of equations," *Mathematical Programming*, vol. 16, pp. 159–176, 1979.